Anal. Chem. **1998,** *70,* 431−437

Accelerated Articles

Counting Single Chromophore Molecules for Ultrasensitive Analysis and Separations on Microchip Devices

Julius C. Fister, III,[†] Stephen C. Jacobson, Lloyd M. Davis,[‡] and J. Michael Ramsey*

Oak Ridge National Laboratory, P.O. Box 2008, Oak Ridge, Tennessee 37831-6142

Separations of 15 pM rhodamine 6G and 30 pM rhodamine B performed in a micromachined electrophoresis channel were detected by counting fluorescence bursts from individual molecules. The migration times, peak widths, and analyte concentrations were estimated from the number and the migration time distribution of the detected molecules. Concentration detection limits estimated at >99% confidence were 1.7 pM rhodamine 6G and 8.5 pM rhodamine B. The separations required <35 s and the relative migration time uncertainties were less than 2.0%. These are the lowest detection limits reported for microchip separation devices and the first example of single-chromophore molecular counting for detection of chemical separations.

Improved techniques for manipulation, separation, and detection of small quantities of dilute reagents would facilitate new applications of single-molecule detection (SMD)[1−12] in fields such as biotechnology,[13,14] ultrasensitive detection, and sensor technology.[15] Microfabricated instruments[16−18] appear to be ideal platforms for developing new ultrasensitive analyses. Monolithic structures that perform enzymatic assays[19] and polymerase chain reactions (PCRs)[20] have been demonstrated. Precolumn[21] and postcolumn[22] reaction chambers have been fabricated to derivatize analytes for fluorescence detection. Also, DNA restriction fragment analysis[23] and PCR amplification with electrophoretic analysis on hybridized[24] and monolithic[25] devices have been reported. However, ultrasensitive detection methods have not been applied to microfabricated devices to fully exploit the advances in microfluidics.

In this work, we report the use of single-molecule fluorescence detection by confocal microscopy for detecting separations of

[†] Present address: University of New Hampshire, Department of Chemistry, Durham, NH 03824.

[‡] Permanent address: University of Tennessee Space Institute, Center for Laser Applications, Tullahoma, TN 37388.

(1) Shera, E. B.; Seitzinger, N. K.; Davis, L. M.; Keller, R. A.; Soper, S. A. *Chem. Phys. Lett.* **1990**, *174*, 553−557.
(2) Keller, R. A.; Ambrose, W. P.; Goodwin, P. M.; Jett, J. H.; Martin, J. C.; Wu, M. *Appl. Spectrosc.* **1996**, *50*, 12A−32A.
(3) Barnes, M. D.; Ng, K. C.; Whitten, W. B.; Ramsey, J. M. *Anal. Chem.* **1993**, *65*, 2360−2365.
(4) Soper, S. A.; Mattingly, Q. L.; Vegunta, P. *Anal. Chem.* **1993,** *63*, 740−747.
(5) Mets, Ü.; Rigler, R. *J. Fluoresc.* **1994**, *4*, 259−264.
(6) Nie, S.; Chiu, D. T.; Zare, R. N. *Science* **1994**, *266*, 1018−1021.
(7) Lee, Y. H.; Maus, R. G; Smith, B. W.; Winefordner, J. D. *Anal. Chem.* **1994**, *66*, 4142−4149.
(8) Mertz, J.; Xu, C.; Webb, W. W. *Opt. Lett.* **1995**, *20*, 2532−2532.
(9) Lermer, N.; Barnes, M. D.; Kung, C.-Y.; Whitten, W. B.; Ramsey, J. M. *Anal. Chem.* **1997**, *69*, 2115−2121.
(10) Nie, S.; Emory, S. R. *Science* **1997**, *275*, 1102−1106.
(11) Castro, A.; Shera, E. B. *Anal. Chem.* **1995**, *67*, 3181−3186.
(12) Li, L. Q.; Davis, L. M. *Appl. Opt.* **1995,** *34*, 3208−3217.
(13) Castro, A.; Shera, E. B. *Appl. Opt.* **1995**, *34*, 3218−3222.
(14) Rigler, R. *J. Biotechnol.* **1995**, *41*, 177−186.
(15) Smith, C. L.; Kricka, L.; Krull, U. J. *Genet. Anal.: Biomol. Eng.* **1995**, *12*, 33−37.
(16) Harrison, D. J.; Manz, A.; Fan, Z.; Lüdi, H.; Widmer, H. M. *Anal. Chem.* **1992**, *64*, 1926−1932.
(17) Harrison, D. J.; Fluri, K.; Seiler, K.; Fan, Z.; Effenhauser, C. S.; Manz, A. *Science* **1993**, *261*, 895−897.
(18) Jacobson, S. C.; Hergenröder, R.; Koutny, L. B.; Warmack, R. J.; Ramsey, J. M. *Anal. Chem.* **1994**, *66*, 1107−1113.
(19) Hadd, A. G.; Raymond, D. E.; Halliwell, J. W.; Jacobson, S. C.; Ramsey, J. M. *Anal. Chem.* **1997**, *69*, 3407−3412.
(20) Wilding, P.; Shoffner, M. A.; Kricka, L. J. *Clin. Chem.* **1994,** *40*, 1815−1818.
(21) Jacobson, S. C.; Hergenröder, R.; Moore, A. W., Jr.; Ramsey, J. M. *Anal. Chem.* **1994**, *66*, 4127−4132.
(22) Jacobson, S. C.; Koutny, L. B.; Hergenröder, R.; Moore, A. W., Jr.; Ramsey, J. M. *Anal. Chem.* **1994**, *66*, 3472−3476.
(23) Jacobson, S. C.; Ramsey, J. M. *Anal. Chem.* **1996**, *68*, 720−723.
(24) Woolley, A. T.; Hadley, D.; Landre, P.; deMello, A. J.; Mathies, R. A.; Northrup, M. A. *Anal. Chem.* **1996**, *68*, 4081−4086.
(25) Waters, L. C.; Jacobson, S. C.; Kroutchinina, N.; Khandurina, J.; Foote, R. S.; Ramsey, J. M. *Anal. Chem.* **1998**, *70*, 158−162.

S0003-2700(97)00724-5 CCC: $15.00
Published on Web 01/01/1998

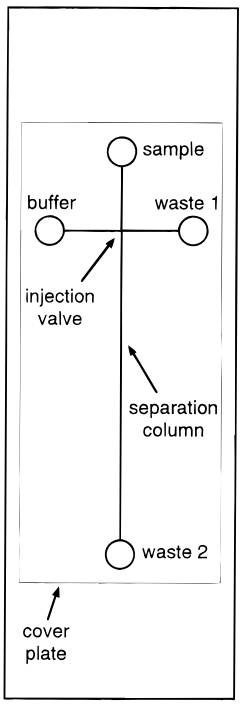

Figure 1. Schematic of microchip.

single chromophore molecules in microfabricated electrophoresis channels. Usually, the migration time, amplitude, and standard deviation of an analyte peak are found by fitting an arrival time distribution to the peak. Unfortunately, when only a few molecules are detected, sampling noise[26] obscures the form of the underlying peak.[27] An additional source of error arises because the intensities of the individual fluorescence bursts are independent of the local analyte concentration; i.e., they are not correlated with the shape of the underlying arrival time distribution. Therefore, in this work, the migration time, the peak variance, and the peak amplitude are derived from the locations and frequency of detected molecules; concentration detection limits are determined by the molecular counting rate compared to the false positive rate.

EXPERIMENTAL SECTION

Microchip Fabrication. Standard photolithographic and wet chemical etching techniques were used to machine a cross-shaped channel network into a glass substrate (Figure 1).[28] The channel dimensions, measured with a surface profiler (Tencor Inc.), were 10.0 μm deep, 48.0 μm wide at the top, and 32.0 μm wide at the bottom; the distance from the injection cross to the probe zone was 13.5 mm. Since the microchip was to be operated with the substrate superior to the channel network, holes were drilled through the substrate to provide access to the channels. A 130-μm thick glass cover slip, which extended over the channel network and holes, was bonded to the machined substrate.[18]

During operation of the microchip, sample solutions were contained in polypropylene pipet tips fit to the drilled holes. The reservoirs were connected to a single high-voltage power supply through a resistive network so that the potential of each reservoir could be controlled independently. Gated injections[22] were performed by using a computer-controlled relay to reduce the potential of the buffer reservoir. The field strength in the separation channel during injections was $\approx$160 V cm^{-1} and during electrophoresis was 210 V cm^{-1}.

Chemicals. The solvent for all experiments was a 50/50 solution of HPLC-grade methanol (Sigma Aldrich) and water (Barnstead Nanopure) which contained 4 mM sodium tetraborate. Rhodamine 6G (R6G) and rhodamine B (RB) (Exciton Inc.) were used as received without further purification. Solutions were prepared immediately before use by multiple dilution in glass bottles.

Fluorescence Detection. The custom-built confocal microscope is similar to those previously described for single-molecule detection.[5,6] The 514-nm output from an argon ion laser (Coherent Innova) operating in single line mode was directed by a dichroic mirror (Omega DM530) into a 100$\times$ 1.3 NA oil immersion objective (Nikon Fluor); the objective focused the laser beam into the separation channel and collected fluorescence. Total internal reflection at the interface between the separation channel and the cover plate limited the actual numerical aperture of fluorescence collection to $\approx$1.2. During operation, the microchip was positioned above the objective and fluorescence excitation and collection was performed through the cover plate and index matching fluid (glycerol). The laser power in the probe zone was estimated to be 540 μW for all experiments. The collected fluorescence was focused onto a 100-μm pinhole positioned at the image plane of the objective. Rayleigh and Raman scattering were rejected with a holographic notch filter (Kaiser Optical, Super Notch) and an interference filter (560 DF40 Omega Optical) placed behind the pinhole. Fluorescence transmitted by the filters was focused by a 2.5-cm focal length plano convex lens onto an actively quenched single photon avalanche diode (SPAD) (EG&G SPCM-AQ-231).

Photon Counting. The SPAD generates a TTL output pulse for 50% of the incident photons. Since spurious afterpulses follow $\approx$1% of the SPAD output pulses, a digital pulse generator (Stanford Research Systems model DG535), set to be nonretriggerable for 200 ns, was used to reject most of the afterpulses.[29] Two counters on a National Instruments counter board, programmed to emulate a multichannel scaler, were used to count output pulses from the pulse generator. To count pulses continually, the counters were read alternately and nondestructively into RAM. This assured that there was no dead time for photon counting bin widths longer than 40 μs. Each data record consisted of 196 608 photon counting bins. The programmable output of a third counter was used to switch the microchip between electrophoresis and injection modes as described above.

RESULTS AND DISCUSSION

To verify that fluorescence signals observed using the confocal microscope described in the Experimental Section are due to individual dye molecules, the dimensions of the effective probe volume and average molecular residence time are characterized via fluorescence autocorrelation spectroscopy. Subsequently, concentration detection limits for single-molecule detection of separations of dilute solutions of laser dyes are evaluated.

Confocal Probe Volume. The focused laser beam and spatial filtering determine the dimensions of the probe zone. Theoreti-

(26) Hungerford, M. J.; Christian, G. D. *Anal. Chem.* **1986**, *58*, 2567−2568.
(27) Chen, D. Y.; Dovichi, N. *Anal. Chem.* **1996**, *68*, 690−696.
(28) Jacobson, S. C.; Hergenröder, R.; Koutny, L. B.; Ramsey, J. M. *Anal. Chem.* **1994**, *66*, 1114−1118.
(29) Spinelli, A.; Davis, L. M.; Dautet, H. *Rev. Sci. Instrum.* **1996**, *67*, 55−61.

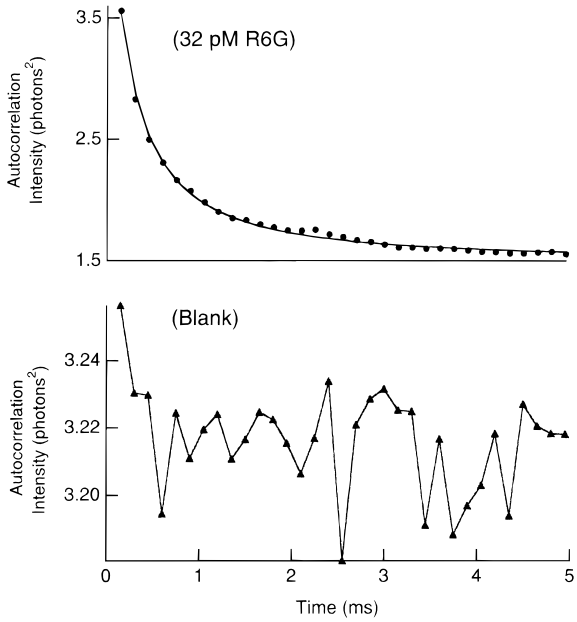

Figure 2. Autocorrelation of diffusion-controlled single-molecule fluorescence in a separation channel. Autocorrelation of fluorescence from 32 pM R6G and blank. Solid line through (●) is the weighted least-squares fit to eq 2 as described in the text; line through (▲) serves only to guide the eye.

cally, for epi-illumination with confocal detection, tight spatial filtering of the collected fluorescence can restrict the full height of the probe volume to <1 μm.[30] In practice, however, spherical aberration increases the effective depth of field.[31−35] Based on the performance of similarly equipped confocal microscopes,[32,33,35] the full $1/e^2$ height of the probe zone is estimated to be $2z_0 = 2.5$ μm. For the 100× objective and 100-μm pinhole used in these experiments, the lateral extent of the probe zone is defined by the $1/e^2$ radius of the laser beam, ω_0, which is ≈0.5 μm for a visible laser beam focused by a high-NA objective. The relative efficiency of excitation and collection within the probe volume, I_p, can be approximated as an ellipsoid with Gaussian profiles in three dimensions[35]

$$I_p = \exp(-2(x^2 + y^2)/{\omega_0}^2) \exp(-2z^2/{z_0}^2) \qquad (1)$$

Although the probe volume dimensions cannot be measured directly, they can be confirmed by fluorescence autocorrelation spectroscopy.[36] To this end, a micromachined separation channel was electrokinetically infused with either a blank or a dye solution and the applied field turned off; i.e., diffusion alone transported molecules into and out of the probe volume. Fluorescence was accumulated immediately into photon counting bins 150 μs wide. Figure 2 shows that the discrete autocorrelation function of the background photocount distribution (neat buffer) is random at offsets >0 s but that the autocorrelation function of fluorescence from a 32 pM R6G solution persists for ≈1 ms due to fluorescence from molecules diffusing through the probe volume.

The autocorrelation function for molecular diffusion through a Gaussian ellipsoid is given by[35]

$$G(t) = A + B\left[1 + \frac{4Dt}{{\omega_0}^2}\right]^{-1}\left[1 + \frac{4Dt}{{z_0}^2}\right]^{-1/2} \qquad (2)$$

where A and B are scaling constants and D is the diffusion coefficient. The scaling constants depend only weakly on the estimated dimensions of the probe volume; in contrast, diffusion coefficients derived from confocal fluorescence correlation spectroscopy are sensitive to both the radius and the height of the probe volume used to fit the data. Therefore, to confirm the probe volume dimensions, eq 2 (with $\omega_0 = 0.5$ μm and $z_0 = 1.25$ μm) was fit to the autocorrelation function by optimizing the constants A, B, and D. The diffusion coefficient estimated from the average of three measurements, $D = 2.7 \pm 0.1 \times 10^{-6}$ cm^2 s^{-1}, agrees to within experimental error with a value of $D = 2.5 \pm 0.3 \times 10^{-6}$ cm^2 s^{-1} determined independently in the same solvent pair by means of a fluorescence correlation spectroscopy approach utilizing patterned excitation of fluorescence.[37] (The latter value is not derived from molecular diffusion through a confocal probe volume.[37]) Using these dimensions, eq 1 predicts that the volume of the probe zone is ≈0.9 fL.

Molecular Residence Time. The average residence time, t_r, of molecules in the probe zone can also be derived from the autocorrelation function. Equating the residence time to the ratio ${\omega_0}^2/4D$, which appears in eq 2, gives $t_r = 230 \pm 30$ μs when diffusion is the only form of mass transport. One might expect that applying a potential across the microchannel would reduce dramatically the molecular residence time. To test this idea, fluorescence from a 32 pM R6G solution was acquired at a field strength of 160 V cm^{-1} corresponding to an electrokinetic velocity of ≈440 μm s^{-1}. The autocorrelation function of these data was characteristic of diffusion-controlled mass transport; the best fit of eq 2 to the autocorrelated data gave a residence time of $t_r = 215 \pm 10$ μs, which is within experimental error of the diffusion controlled residence time.

Single-Molecule Detection Following Injection of Dilute R6G Solutions. Figure 3 shows electropherograms acquired from a blank and from solutions containing 6 and 32 pM R6G. The measured electrokinetic velocity of rhodamine 6G in electrophoresis mode was 585 μm s^{-1}; during injections, the velocity was ≈25% less. The volume of the 2-s gated injections, estimated from the electrokinetic velocity and channel geometry, was ≈330 pL. Using the confocal microscope described above, photons were accumulated into 150-μs-wide bins. For clarity, only one of four replicates is shown and electropherograms from solutions containing 12, 18, and 25 pM R6G are not shown. Groups of intense fluorescence bursts, distinct from the average background, occur with a migration time of ≈23 s for each analyte injection. Figure 4 shows an expanded region of these data, 200 ms wide, to illustrate the high S/N associated with fluorescence from R6G molecules entering the probe volume.

One criterion for establishing that the fluorescence bursts are due to individual molecules entering the probe volume is a

(30) Shepard, C. J. R. *J. Microsc.* **1988**, *149*, 73−75.
(31) Qiang, H.; Elson, E. L. *Appl. Opt.* **1991**, *30*, 1185.
(32) Palmer, A. G., III; Thompson, N. L. *Appl. Opt.* **1989**, *28*, 1214−1220.
(33) Schneider, M. B.; Webb, W. W. *Appl. Opt.* **1981**, *20*, 1382−1388.
(34) Rigler, R.; Mets, Ü. *J. Eur. Biophys.* **1993**, *22*, 169−175.
(35) Aragón, S. R.; Pecora, R. *J. Chem. Phys.* **1976**, *64*, 1791−1803.
(36) Elson, E.; Magde, D. *Biopolymer* **1974**, *13*, 1−29.
(37) Hansen, R. L.; Zhu, X. R.; Harris, J. M. *Anal. Chem.*, submitted.

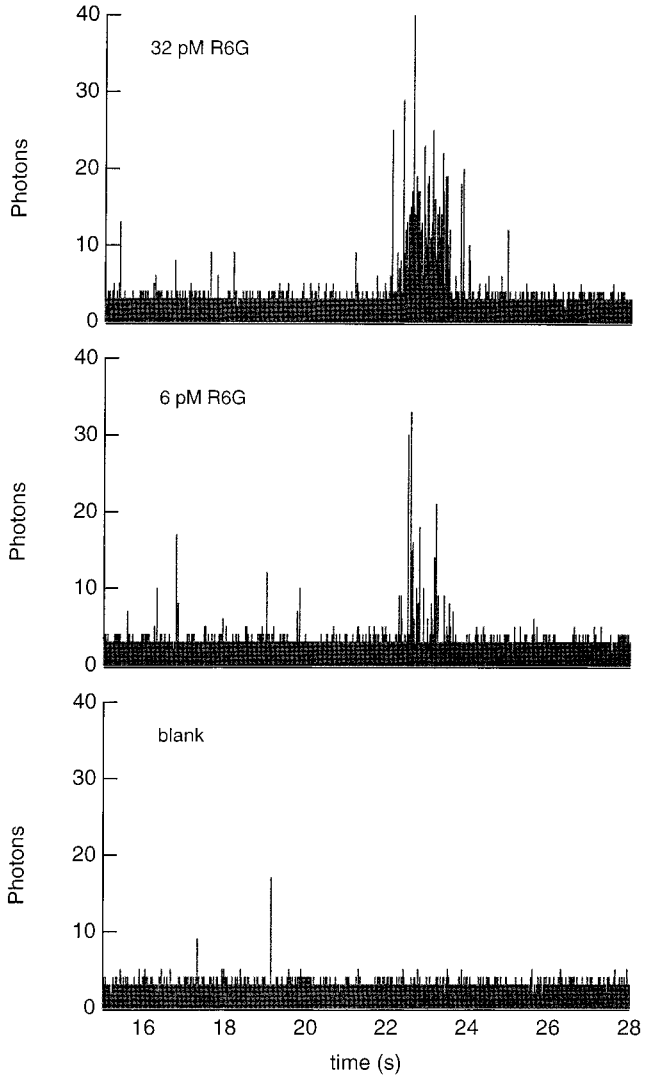

Figure 3. Single-molecule detection of R6G. Raw data from 2-s gated injections of solutions containing 32 pM, 6 pM, and blank. Photon counting bin width, 150 μs.

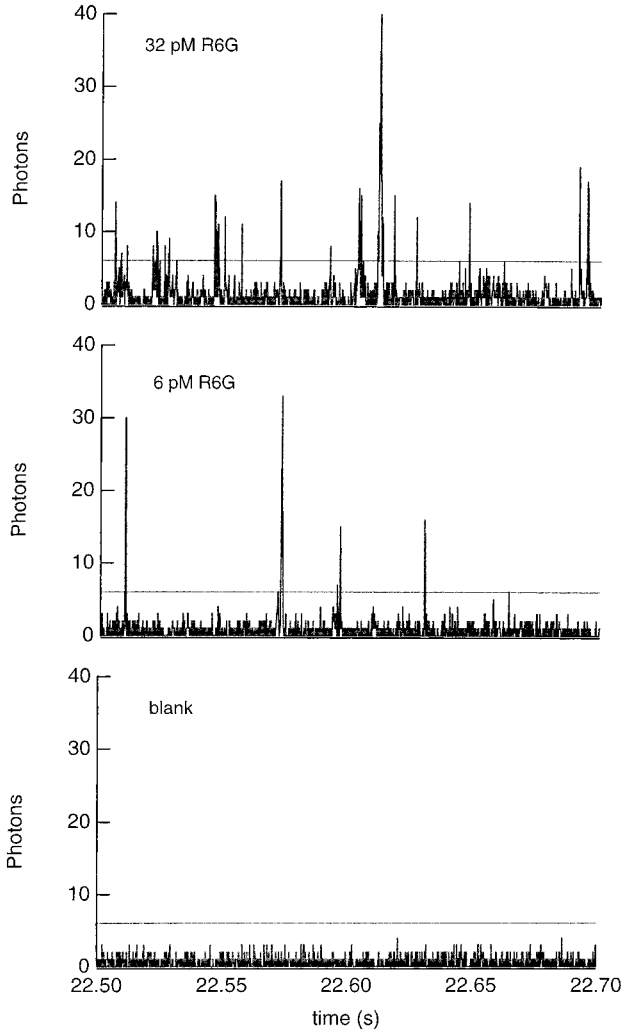

Figure 4. Expanded 200-ms region of data from Figure 2. The solid lines correspond to a molecular detection threshold of ≥6 photons.

negligible probability that >1 molecule enters during a given photon counting interval. If the photon counting bin width is short compared to the average molecular residence time, the mean number of molecules that sample the probe zone during a given photon counting interval will be approximately equal to the product of the probe volume and the concentration. The average residence time determined from the autocorrelation analysis presented above is >25% longer than the photon counting bin width used to acquire the data in Figure 3. Therefore, based on the 0.9-fL confocal probe volume, the average molecular occupancy for the most concentrated solution (32 pM) is 0.017. An analysis using Poisson statistics predicts that <1% of the fluorescence bursts in Figure 3 is attributable to the presence of >1 molecule in the probe volume.

If successive molecules enter the probe zone in a discrete, random fashion, a distribution of time intervals between detected molecules would be characterized by a single, decaying exponential.[38,39] In free solution, however, a 3D random walk model predicts that ≈35% of freely diffusing molecules re-enter the probe volume.[40] Re-entries increase the molecular count rate and bias the distribution of waiting intervals toward shorter intervals.[39] The waiting time distribution between fluorescence bursts exceeding a 5-photon count threshold derived from the fluorescence of 32 pM R6G acquired at an electrokinetic velocity of ≈440 μm s^{-1} is shown in Figure 5. The average detection interval, determined from an exponential fit to long intervals, is 14 ± 0.6 ms; whereas, the deviation from exponential behavior persists to only ≈3.5 ms. Therefore, although some molecules rapidly re-enter the probe zone, *successive* molecules arrive randomly. The relative difference between the data and the exponential fit in Figure 5 shows that re-entering molecules increase the molecular count rate by ≈20%, as indicated by the area represented by the difference between the experimental data and the exponential fit at shorter waiting intervals, e.g., <3 ms. These observations combined with the autocorrelation analysis discussed earlier indicate that diffusion-controlled mass transport strongly controls the molecular detection rate. The use of electrokinetic mass transport ensures that the population of dye molecules surrounding the probe volume

(38) Kung, C.-Y.; Barnes, M. D.; Lermer, N.; Whitten, W. B.; Ramsey, J. M. *Anal. Chem.* **1998**, *70*, 658−661.

(39) Chiu, D. T.; Zare, R. N. *J. Am. Chem. Soc.* **1996**, *118*, 6512−6513.

(40) McCrea, W. H.; Whipple, F. J. W. *Proc. R. Soc Edinburgh* **1940**, *60*, 281−298.

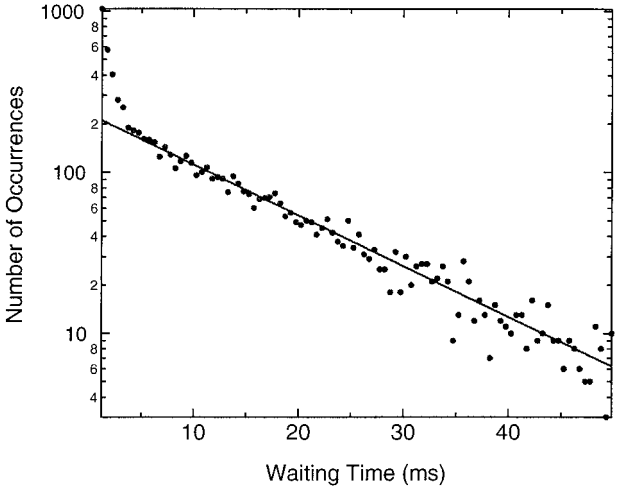

Figure 5. Histogram of waiting times (●) derived from single-molecule detection of 32 pM R6G in a separation channel at ≈160 V cm^{-1}. Solid line through points is a weighted exponential fit to waiting times of ≥3.75 ms.

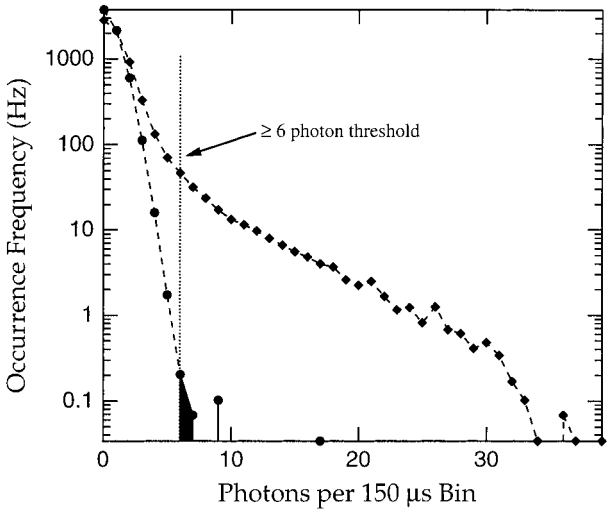

Figure 6. Histogram of photocount distributions for 32 pM R6G (◆) and blank (●). The 6-photon threshold is indicated with the dashed line, and false positives are shaded. The data are generated by continuous infusion of the solution using a field strength of 175 V cm^{-1}.

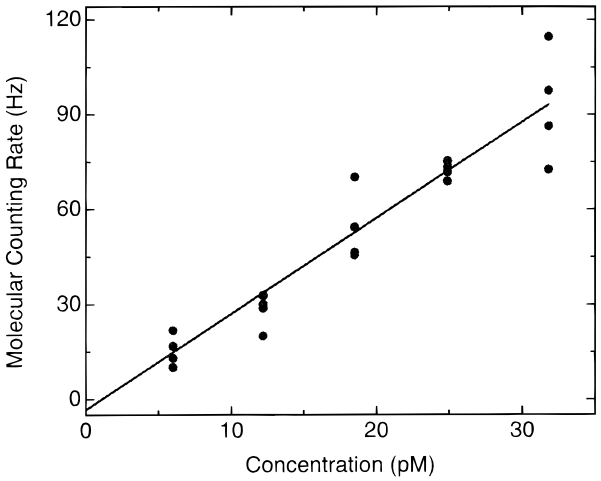

Figure 7. Calibration curve of the number of molecules detected in 1-s windows about the peak maximums in Figure 3 versus concentration. Solid line is the best-fit weighted least squares. The slope and intercept are 3.1 ± 0.2 molecules pM^{-1} s^{-1} and −3.5 ± 2.4 molecules, respectively.

is not depleted by photobleaching but does not increase significantly the molecular counting rate.

Analyte Detection. The intense photon bursts in Figures 3 and 4 satisfy important criteria for single-molecule fluorescence detection: the probability of multiple occupancy is negligible and successive molecules enter the probe volume in random fashion. In most applications of single-molecule detection, a molecular detection threshold discriminates individual fluorescence bursts from fluctuations in the background photocount distribution. Unfortunately, since intense bursts also appear in blank solutions, the presence of an analyte due to an injection cannot be declared upon observing an individual fluorescence burst signal. (Several of these false positives are evident in the blank shown in Figure 3 between 15 and 20 s when no sample is expected.) The presence of an analyte peak can be declared only when the local molecular detection rate exceeds that expected for the false positive rate. The optimum molecular detection threshold, therefore, maximizes the ability to discriminate between fluctuations in the false positive rate and the actual molecular detection rate at low analyte concentrations; the optimal molecular detection threshold is found by evaluating both the photocount distributions and molecular detection rates for blanks and analyte injections.

In Figure 6, the photocount distributions for a solution containing 32 pM R6G and a blank solution are depicted. For blank samples, the distribution of photon counting bins containing ≤5 photons was Poissonian with a mean of 0.565 ± 0.002 photon/bin. (The uncertainty of the mean background represents the precision with which the mean is known, not the standard deviation of the photocount distribution.) However, because of fluorescent impurities in the methanol or buffer, there were more bins containing ≥6 photons than predicted. Since the photocount distributions of the impurity and analyte molecules were similar, raising the threshold above 6 photons did not discriminate impurity molecules from analyte molecules; at lower thresholds, fluctuations in the average background increased the false positive rate dramatically. At a threshold of ≥6 photons/bin, the average false positive rate was only 0.56 s^{-1} (shaded area in Figure 6) representing a >99.99% confidence level for distinguishing individual fluorescence bursts from the background photocount distribution.

Since the axial extent of the injections in Figure 3 is wide relative to diffusion or other broadening mechanisms, the R6G population at the plateaus of the peaks is not depleted significantly during electrophoresis. Therefore, the absolute molecular detection rate for low analyte concentrations was estimated from the maximum number of molecules detected in 1-s windows about the centers of the peaks and plotted as a function of concentration as shown in Figure 7. Although pulse pileup would cause the molecular detection rate to saturate at higher concentrations,[27] a linear fit to the data in Figure 7 is appropriate because of the low average occupancies. For a molecular detection threshold of ≥6 photons/bin, the molecular detection rate estimated from the slope of the calibration line is 3.1 ± 0.2 molecules pM^{-1} s^{-1} and the intercept of −3.5 ± 2.4 molecules is indistinguishable from zero at 95% confidence.

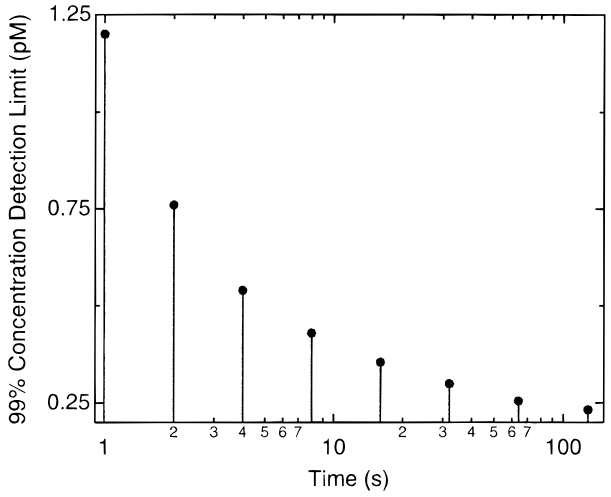

Figure 8. The >99% concentration detection limit for R6G as a function of time. Points are calculated from Poissonian confidence limits as described in the text.

Given the false positive rate of 0.56 s^{-1}, Poisson statistics predict that when 4 molecules are detected within 1 s the presence of an analyte can be declared with >99.7% confidence. Based on the molecular detection rate of 3.1 ± 0.2 molecules pM^{-1} s^{-1}, this corresponds to a concentration detection limit of 1.2 pM R6G. This concentration detection limit was lower than that predicted for other molecular detection thresholds; i.e., the concentration detection limit as a function of the molecular detection threshold exhibited a minimum at a threshold of 6 photons/bin.

Single-molecule detection is most advantageous for lowering detection limits when a sample can be observed for longer time periods; concentration detection limits for longer counting periods can be predicted using the absolute molecular detection rate determined above. Figure 8 predicts that a detection limit of <250 fM R6G is achievable after only 2 min of continuous molecular counting. Since the concentration detection limits are calculated from Poisson confidence intervals, Figure 8 presents the predicted detection limit versus observation time in discrete steps rather than as a smooth function.

The total molecular detection efficiency of the instrument can be calculated from the ratio of the slope of the calibration curve (3.1 molecules pM^{-1} s^{-1}) to the estimated flux of molecules passing the probe volume. Given the electrokinetic velocity of 585 μm s^{-1} and the height (10 μm) and average width (40 μm) of the separation channel, the flux of molecules passing a plane containing the probe zone is estimated to be 141 molecules pM^{-1} s^{-1}. After correcting for the 20% of counts due to recounted molecules, the total molecular detection efficiency is estimated to be 1.75%. Because diffusion is the dominant source of mass transport over short distances, the detection efficiency is ≈3× larger than predicted by taking the ratio of the cross-sectional areas of the probe zone and the channel.

Separations. Single-molecule counting for detection of separations was evaluated using ≈200-pL injections (1.25-s injection duration) of a solution containing 15 pM R6G and 30 pM RB; fluorescence was accumulated into 200 μs photon counting bins. Figure 9a shows the raw data for one of three replicates. For clarity, only a 15-s region containing the peaks is shown.

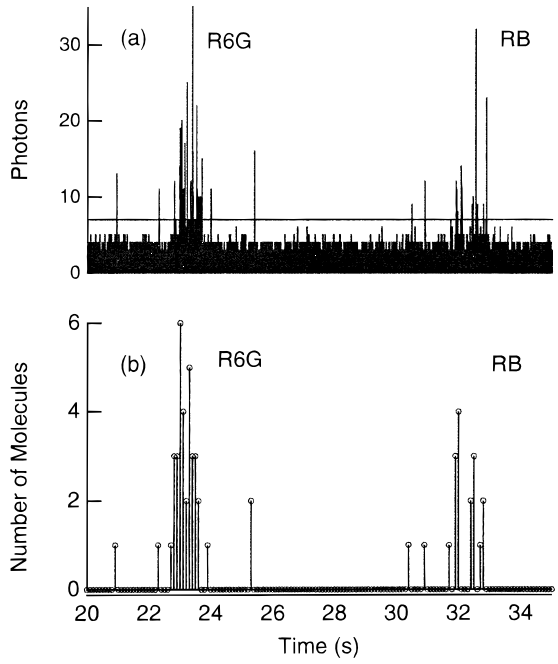

Figure 9. Separation of R6G and RB. (a) Raw data from a 1.25-s gated injection of a solution containing 15 pM R6G and 30 pM RB. Solid line represents a molecular detection threshold of ≥7 photons/bin. (b) Histogram of the number of molecules detected in 100-ms-wide intervals.

To select a molecular detection threshold, the electropherograms were processed as described above. The average background of 0.791 ± 0.003 photon/bin in these data was higher because of the increased photon counting bin width. For the optimal molecular detection threshold of ≥7 photons, the average false positive rate was 0.3 s^{-1}.

To illustrate the deterioration of peak shape when only a few molecules are detected, Figure 9b shows the number of molecules detected in consecutive 100-ms windows along the electropherogram. (The 100-ms window was chosen to contrast the peak shape distribution of R6G at ≈23 s with that of RB at ≈32 s and yet be narrow relative to the peak shape distributions.) Despite the loss of peak shape, the parameters that define the underlying peaks, i.e., the amplitude, the migration time, and the standard deviation, can be inferred from the distribution of detected molecules. To locate and count the majority of molecules associated with each analyte peak yet avoid counting excess impurity molecules, the electropherograms should be searched for groups of detected molecules using a molecular counting window equal to the expected full width of the analyte peaks.

In Figure 9a, the standard deviation of the underlying peaks, σ_p, is dominated by contributions from diffusion, σ_D, and the injection length, σ_{inj}:

$$\sigma_p = (\sigma_{inj}^2 + \sigma_D^2)^{1/2} = \left(\frac{t_{inj}^2}{12} + 2Dt/v^2\right)^{1/2} \quad (3)$$

where t_{inj} is the injection duration, D is the diffusion coefficient, t is the mean migration time, and v is the mean analyte velocity. The standard deviation due to the injection, after a correction for the reduced field strength during injection, is $\sigma_{inj} \approx 0.25$ s. The

diffusion coefficient of R6G derived from the fluorescence autocorrelation function and the mean electrokinetic velocity of 500 μm s^{-1} lead to $\sigma_D \approx 0.25$ s. Therefore, the predicted standard deviation of the underlying peaks is $\sigma_p \approx 0.35$ s, and the full width, given by 4 σ_p, is 1.4 s.

Given the predicted full width of the underlying peaks and the average false positive rate of 0.3 s^{-1}, the >99% confidence analyte detection threshold is ≥3 molecules in 1.4 s. When the data were searched for 1.4-s regions containing ≥3 molecules, two maximums were found within each electropherogram. The average migration time of molecules within the 1.4-s windows was 22.9 ± 0.2 s for R6G and 31.8 ± 0.6 s for RB and an average of 32 ± 6 R6G molecules and 13 ± 5 RB molecules were detected. A single spurious peak containing 3 molecules occurred in one of the electropherograms.

The mean standard deviations of the molecular migration time distributions derived from three injections were indistinguishable from the predicted value of $\sigma_p \approx 0.35$ s and the relative migration time uncertainty of both analytes was <2%. However, consistent with the detection of 2.5 times more R6G molecules as RB molecules, the relative precision of the average migration time and the number of detected molecules was higher for R6G.[27]

Concentration detection limits, estimated at >99% confidence from the average number of detected molecules, were 1.7 pM R6G and 8.5 pM RB. The R6G detection limit is slightly higher than that predicted for a 1.4-s counting interval from the calibration curve in Figure 7 because the duration of the sample injection, after correcting for the reduced electrokinetic velocity, was only ≈0.9 s. The lower sensitivity of RB relative to R6G stems from a smaller absorption cross section at 514 nm so that fewer photons are emitted and detected.

Although stochastic fluctuations in the number of detected molecules[26] limit precision near the concentration detection limit, precision could be improved by performing multiple injections. For example, the relative precision in the average number of molecules detected from 1.25-s injections of 30 pM RB was ≈40%. If 20 sequential samples were injected (which would require only 10 min), the relative uncertainty in the number of detected molecules would be <10%. A similar improvement would be realized for the peak width uncertainty. Performing multiplexed injections, as in correlation chromatography,[41] provides similar benefits with reduced analysis times.

CONCLUSION

The sensitivity and precision achieved in these experiments is sufficient to indicate a number of possibilities for ultrasensitive analyses on microfabricated structures. For example, immunoassays for subpicomolar concentrations of a target molecule would require only a few nanoliters of sample. The ability to manipulate small volumes of fluid could be exploited in fluorescence correlation spectroscopy to mix target molecules with different reagents and transport them sequentially to the detection zone. Chemical reactions generating minute quantities of fluorescent products could be analyzed either continuously or serially to monitor the concentration of the product(s).

Although only ≈1.75% of the injected molecules is detected in the current configuration, several improvements could significantly increase this figure. Machining a separation channel 5 μm deep and 5 μm wide would reduce the cross-sectional area of the sample stream by a factor of ≈15. Since channel dimensions of 5 × 5 μm would be significantly larger than the confocal probe volume, the background due to scattering from the substrate−channel interface would not increase significantly. Therefore, the fraction of injected molecules detectable could exceed 20%.

Sample stream widths of only 3.3 μm are achievable by means of electrokinetic focusing.[42] In addition to sample confinement, concentration enhancement can be obtained in the focused analyte stream by employing sample stacking techniques. If multiple photolithographic steps were employed in the fabrication process, a sample stream could be tightly confined in two dimensions, which would allow total detection efficiencies to approach 75%.[12]

High molecular detection efficiencies could also be achieved if a microchannel network was coupled to a piezoelectric droplet generator;[38] single-molecule fluorescence would be detected off-chip in a stream of microdroplets. In this manner, the total content of a microfabricated reaction chamber or the eluent from a separation channel could be sequentially analyzed in a digital fashion.[43]

ACKNOWLEDGMENT

This research was sponsored by the Department of Energy, Office of Research and Development. Oak Ridge National Laboratory is managed by Lockheed Martin Research Corp. for the U.S. Department of Energy, under Contract DE-ACO5-96OR22464. This research was sponsored in part by appointments for J.C.F. to the ORNL Postdoctoral Research Associates Program and for L.M.D. to the Visiting Faculty Research Participation Program, which are administered jointly by the Oak Ridge Institute for Science and Education and ORNL. We thank Justin E. Daler for fabrication of the microchips. The authors thank Chung-Yi Kung, Michael D. Barnes, Richard Hansen, John W. Halliwell, and Noah N. Lermer for helpful discussions and (C.-Y.K.) for programming assistance.

Received for review July 7, 1997. Accepted December 1, 1997.

AC9707242

(41) Smit, H. C. *Chromatographia* **1970**, *3*, 515−518.
(42) Jacobson, S. C.; Ramsey, J. M. *Anal. Chem.* **1997**, *69*, 3212−3217.
(43) Ng. K. C.; Whitten, W. B.; Arnold, S.; Ramsey, J. M. *Anal. Chem.* **1992**, *64*, 2914−2919.